Microporous and Mesoporous Materials 226 (2016) 243–250

Contents lists available at ScienceDirect

Microporous and Mesoporous Materials

journal homepage: www.elsevier.com/locate/micromeso

Controlled delivery of drugs adsorbed onto porous Fe_3O_4 structures by application of AC/DC magnetic fields

Mislav Mustapić [a, g, *], Md Shahriar Al Hossain [a, **], Joseph Horvat [a], Pawel Wagner [b], David R.G. Mitchell [c], Jung Ho Kim [a], Gursel Alici [d], Yoshitaka Nakayama [e], Boris Martinac [e, f]

[a] Institute for Superconducting and Electronic Material (ISEM), University of Wollongong, Squires Way, North Wollongong, NSW 2522, Australia
[b] Intelligent Polymer Research Institute/AIIM Faculty Innovation Campus, Squires Way, University of Wollongong, NSW 2522, Australia
[c] Electron Microscopy Centre/AIIM Faculty Innovation Campus, Squires Way, University of Wollongong, NSW 2522, Australia
[d] School of Mechanical, Materials and Mechatronic Engineering and ARC Centre of Excellence for Electromaterials Science, University of Wollongong, NSW, 2522, Australia
[e] Molecular Cardiology and Biophysics Division, Victor Chang Cardiac Research Institute, NSW 2010, Australia
[f] St Vincent's Clinical School, University of New South Wales, Darlinghurst, NSW 2010, Australia
[g] University of Osijek, Department of Physics, Trg Ljudevita Gaja 6, Osijek, Croatia

ARTICLE INFO

Article history:
Received 7 August 2015
Received in revised form
27 November 2015
Accepted 14 December 2015
Available online 30 December 2015

Keywords:
Drug delivery
Porous Fe_3O_4
Magnetic fields
Methyl blue
Superparamagnetic

ABSTRACT

Porous structures made up of Fe_3O_4 nanoparticles were used to adsorb methyl blue in water. Controlled release of the methyl blue to water was then achieved by application of a magnetic field. Application of a pure DC field did not result in any release. Application of a pure AC field caused released of the methyl blue. However, a combination of both DC and AC fields resulted in much faster release. The mechanism by which this operated is believed to result from viscous friction. Nanoparticles are strongly aligned in the DC field and oscillate under the influence of the AC field. This study demonstrates a concept for controlled drug delivery, where pharmaceutical molecules, similar to methyl blue, would be adsorbed onto porous Fe_3O_4 structure and the released at a target by application of appropriately localised magnetic fields.

1. Introduction

Design and construction of a complete drug delivery system, from a drug nano-carrier to an efficient system for drug activation in a localised volume of the human body requires a multidisciplinary approach and substantial investment. Selection of proper drug-carriers from various candidates such as liposomes [1–3], nanoparticles, porous materials [4–8], polymer-drug conjugates [9–11], protein (albumin) nanoparticles [12–14], polymeric micelles [15–17], is the first part of this effort. Porous materials possess a large surface area and so have the capability to store different molecules (drugs) within this structure making them potential drug carriers.

In this paper we demonstrate that porous Fe_3O_4 structures can be used as a vehicle for the transport of drugs adsorbed onto their porous surface. This material enables controlled release of the chemical payload via activation by a magnetic field. We used methyl blue as a surrogate drug. It adsorbs onto the Fe_3O_4 surface, and its release into the surrounding water via application of a magnetic field that can be monitored quite readily by measuring the light absorption through water. This is a proof of the concept that organic molecules can be adsorbed onto an Fe_3O_4 carrier and the release thereof controlled by an external stimulus (applied magnetic field).

Methyl blue is a common biological dye, as is methylene blue, one of the first synthetic drugs. These dyes attach to the tissues through electrostatic interaction. We believe the same mechanism is responsible for the loading of methyl blue onto our porous Fe_3O_4 structures. Drugs that are electrically charged when dissolved in water are likely candidates for loading into the Fe_3O_4 structures.

* Corresponding author. University of Osijek, Department of Physics, Trg Ljudevita Gaja 6, Osijek, Croatia. Tel.: +385 976336964.
** Corresponding author. Tel.: +61 4221 3384.
E-mail addresses: mislav.mustapic@gmail.com (M. Mustapić), shahriar@uow.edu.au (M.S. Al Hossain).

http://dx.doi.org/10.1016/j.micromeso.2015.12.032
1387-1811/

Furthermore, a great advantage of Fe_3O_4 nanoparticles is their biological compatibility [18–20]. Such an important feature enables the use of the nanoparticles without a requirement for biologically tolerable coatings, which might otherwise degrade their saturation magnetization and drug absorption ability.

2. Methods and experiments

2.1. Synthesis of Fe_3O_4 nanoparticles

Magnetite nanoparticles were synthesised with a wet technique by forming a micro-emulsion solution, similar to that used in our previous work [21,19]. Iron sources used were iron (II) chloride and iron (III) chloride dissolved in deionised (DI) water in separate beakers in a molar ratio of 1:2. The solution with iron (II) ions was maintained under an argon atmosphere to eliminate oxidation to iron (III). Both solutions were stirred for half an hour. The micro-emulsion Me1 was prepared in the third beaker.

The micro-emulsion Me1 used in this research consisted of cyclohexane (organic solvent), cationic surfactant hexadecyltrimethylammonium bromide (CTAB), and anionic surfactant sodium dodecyl sulfate (SDS). A combination of two different polarity types of surfactants is required because of the possible formation of larger vacancies inside Fe_3O_4 samples (attraction between them), as well as creation of bilayer vesicles.

In the next step the micro-emulsion Me1 and solution of Fe^{3+} were added to a solution of Fe^{2+} maintained in argon to form the micro-emulsion Me2. Shortly after that, 30w% ammonium solution was added from a separation funnel to Me2. The formation of black particles started immediately upon adding the ammonium solution.

Black powders were collected and washed several times with DI water and acetone and dried overnight. Next day the dried black powders were heated in a furnace at 250 °C for 2 h in a protective argon atmosphere.

2.2. Structural characterization

TEM imaging was performed using a probe-corrected JEOL ARM200F equipped with a cold field emission gun and a Gatan UltraScan CCD. The microscope was also equipped with a JEOL large area EDS detector with collection angle of ~1 sr. The black powder sample was suspended in an emulsion of water and cyclohexane, centrifuged, and drop-cast on a Holey carbon Cu grid for TEM/STEM observation. All imaging and analysis was carried out using 200 kV electrons.

X-ray powder diffraction (XRD) was carried out on a Philips diffractometer, model PW1820 (Cu K_α radiation), in Bragg–-Brentano geometry.

ASAP2000 (Micromeritics, USA) gas sorption analyser was used to determine the adsorption/desorption isotherm, specific surface area and pore size distribution of the sample. Pre-weighed powders were degassed at 300 °C to a residual pressure of 6.67 Pa. Analysis was then performed using N_2 as the adsorbate at 77 K.

2.3. Magnetic measurement

Magnetic measurements on nanoparticles were performed using a Quantum Design MPMS-5T SQUID magnetometer. Magnetic hysteresis loops M(H) were measured in an applied field within a range of 2 T at three different temperatures (10 K, 100 K, and 310 K) temperatures.

2.4. Cytotoxicity test of the Fe_3O_4

The cultures of A549 human lung cancer cells and trypan blue stain have been used in cytotoxicity experiments. Detailed description of cytotoxicity experiments has been reported in our previous work. Similar to our previous work with $CoFe_2O_4$ nanoparticles [21], the cells from all the cultures with porous Fe_3O_4 exhibited negligible cytotoxicity with cell viability ranging close to the blank culture, as can be seen in Fig. 1b.

2.5. AC/DC magnetic field testing

The experimental testing system was made from simple components as shown in Fig. 2. A commercial permanent magnet (rare earth) was placed on the top of the setup. A bottle containing porous magnetic particles and methyl blue dye was dispersed in a water solution. The AC magnet made from 750 turns of copper wire wrapped on a permalloy core. This was positioned below the bottle. The copper coil was plugged in a signal generator GFG-2000/2100 delivering alternating current of up to 100 mA. The distance between the two magnets (Nd–Fe–B and AC) was 7 cm.

Magnetic Fe_3O_4 nanoparticles were soaked in 0.001 M solution of methylene blue (MB) and left overnight to saturate. The nanoparticles were separated from MB solution using permanent magnet and washed several times with DI water. This removed any loosely bound MB, but retained MB within the pores, prior to the application of the magnetic field.

3. Results and discussion

3.1. SEM and TEM analysis

Imaging and diffraction were carried out in conventional TEM mode. Scanning TEM (STEM) was also used, imaging in high angle annular dark field (HAADF), bright field and secondary electron modes. Fig. 3(a,b) are STEM secondary electron images which show agglomeration of roughly spherical particles with particle diameters in the range 10–30 nm. SEM secondary electron imaging (Fig. 3c,d) showed micron-sized agglomerates with a porosity at the 100 nm scale. The agglomerates show extensive porosity, ranging pores from 100 nm down to interparticle porosity at less than the particle diameter. To understand this fine scale porosity, TEM was used.

The TEM images show internal porosity within individual crystallites. Such porosity often forms when low temperature (often amorphous or poorly crystalline) phases densify during heat treatment or crystallisation at higher temperature [22]. The pores are 3–5 nm in diameter and show strong faceting. Typically, the internal surfaces of voids are bounded by the densest (low index) planes, such as {100}, {110} and {111} in order to minimise surface energy. This is also true for the external facets of the crystal. The faceting will depend on the crystal structure. The vast majority of these voids are completely internal, since the SE images (Fig. 3a, b) do not show any cratering or puckering, where such voids intersect the surface. In fact, during heat treatment the external surface would reconstruct to minimise the additional surface area induced by a surface-breaking voids. Internal porosity will be fully closed and will not be accessible to MB impregnation and porosimetry measurements.

The inset diffraction pattern in Fig. 4 shows the material to be strongly crystalline. The spotty rings reflect the large number of randomly oriented particles within the field of view from which this pattern was obtained. The pattern contained large bright reflections and more diffuse weak reflections (of similar spacing). The former originated from the largest crystallites (ca 50 nm in diameter), while the latter arose from the very smallest crystals

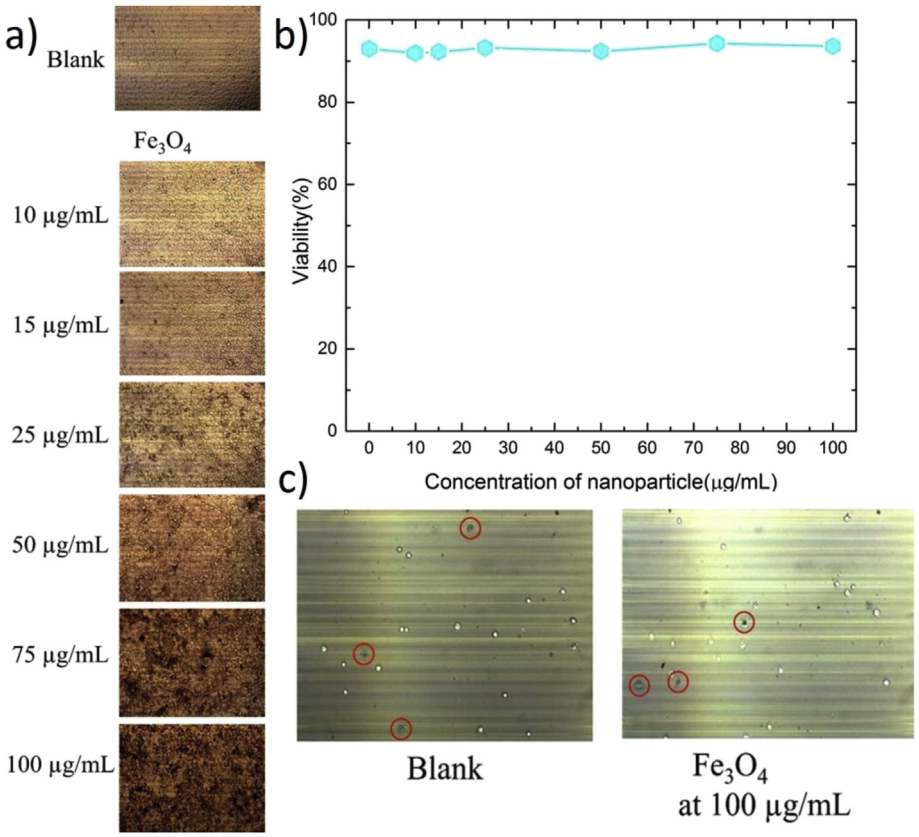

Fig. 1. Cytotoxicity of the Fe_3O_4 sample. a) Images of cells in culture with an increasing concentration of the Fe_3O_4; b) cell viability in different concentrations of the nanoparticles; c) cells after staining with trypan blue showing uncoloured alive cells and blue dead cells. (For interpretation of the references to colour in this figure legend, the reader is referred to the web version of this article.)

(ca10 nm). The d-spacings obtained from the pattern showed these results: 0.490, 0.300, 0.257, 0.215, 0.175, 0.164, 0.150, 0.131, 0.122, 0.111, 0.108, 0.100 nm, and they are in good agreement with XRD measurements (JCPDS data for magnetite – below).

3.2. Porosimetry analysis

Specific surface areas were calculated using Brunauer–Emmet–Teller (BET) model [23] from a linear part of BET

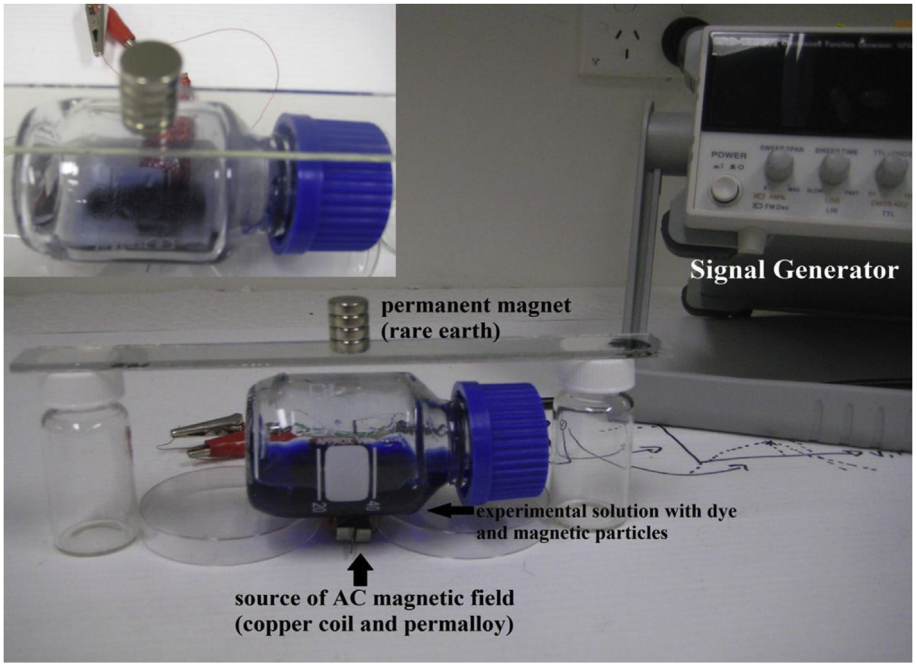

Fig. 2. Experimental apparatus showing how AC and DC magnetic fields were applied.

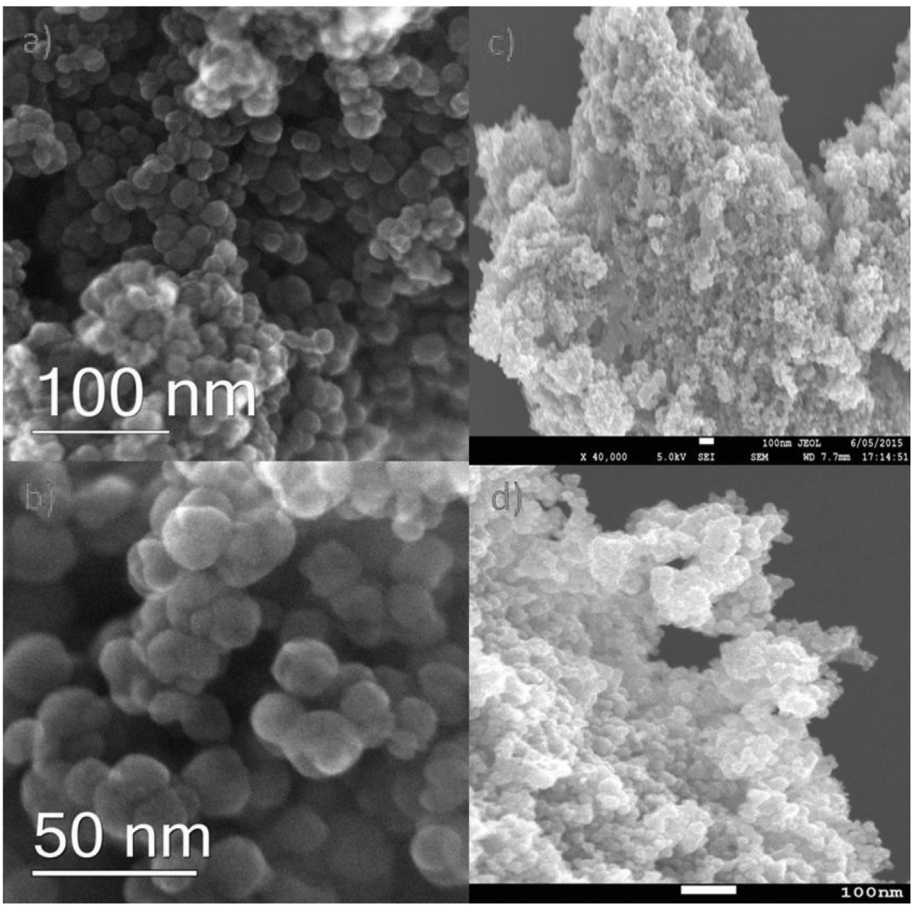

Fig. 3. Secondary electron (SE) images of Fe_3O_4 nanoparticles: a) STEM SE image of the surface of an agglomerate composed of 10–30 nm diameter particles; b) Detail of a) showing the smooth, rounded particles with extensive open porosity; c) and d) SEM images showing porosity at up to 100 nm.

plot. The value obtained for the Fe_3O_4 porous particles was 11.22 m^2/g. Pore size distribution was calculated from the adsorption branch of isotherm by using Barrett–Joyner–Halenda (BJH) model [24]. According to our calculations the pore size distribution is in a range between 5 and 150 nm, with the vast majority ranging between 10 and 50 nm (average pore diameter 10,7 nm), which is in good agreement with the SEM results (Figs. 5 and 6).

Considering all specified data we can conclude that examined Fe_3O_4 samples according to IUPAC classification can be characterised as a macro-porous material. Pores smaller than 2 nm have not been observed in porosimetry analysis.

3.3. XRD analysis

X-ray diffraction (XRD) pattern of porous Fe_3O_4 is presented in Fig. 7. All indexed peaks belong to the spinel structure of magnetite. A good match was obtained with the standard XRD pattern for magnetite (JCPDS, File No. 00-002-1054), and no other phases were detected. Sharp peaks indicate high crystallinity of the sample in good agreement with the TEM analysis.

3.4. Magnetic measurements

Fig. 8 presents the magnetic hysteresis loops of porous Fe_3O_4 at three different temperatures. The S-shaped hysteresis loops with negligible coercive field (H_C) are a typical feature of superparamagnetic nanoparticles and the results are similar to our previous work on Fe_3O_4 nanoparticles [21,19,25,26]. Application of a magnetic field aligns the magnetic moments of the nanoparticles and the magnetization of the sample was almost completely saturated at less than 5000 Oe.

The saturation moment (M_S) measured at 10 K is quite high and has a value of 85.5 emu g^{-1}, while at 310 K the saturation moment was slightly smaller at around 77 emu g^{-1}. These values are comparable to bulk Fe_3O_4, with M_S of 92 emu g^{-1} at T = 10 K [29]. S-shaped magnetic hysteresis loops and small coercive fields were also obtained for nanoparticle Fe_3O_4 reported elsewhere [27–30], despite the much greater particle size in porous samples prepared here.

The lower M_S of nanoparticles, as compared to larger crystals, occurred because magnetic ordering was suppressed in a thin surface layer, where the crystal order is suppressed by defects. The ratio of the surface layer thickness to particle radius increased as the particle size decreased. This resulted in a relatively large proportion of magnetically and crystallographically disordered volume, when compared to the bulk samples [31]. Therefore, M_S became smaller than for the bulk crystal. Small H_C values were obtained for the nanoparticulate material, because the magnetic moment of each nanocrystallite making up this material was small enough to become perturbed by thermal excitation. There are no magnetic domains in such small nanocrystallites. An applied magnetic field easily rotates the magnetic moments and irreversibility effects and H_C occur because of weak interaction between neighbouring nanocrystallites.

3.5. FT-IR measurements

Most of the vibrations observed in Fig. 9 are attributed to the bonds in aromatic rings related to methyl blue. According to the

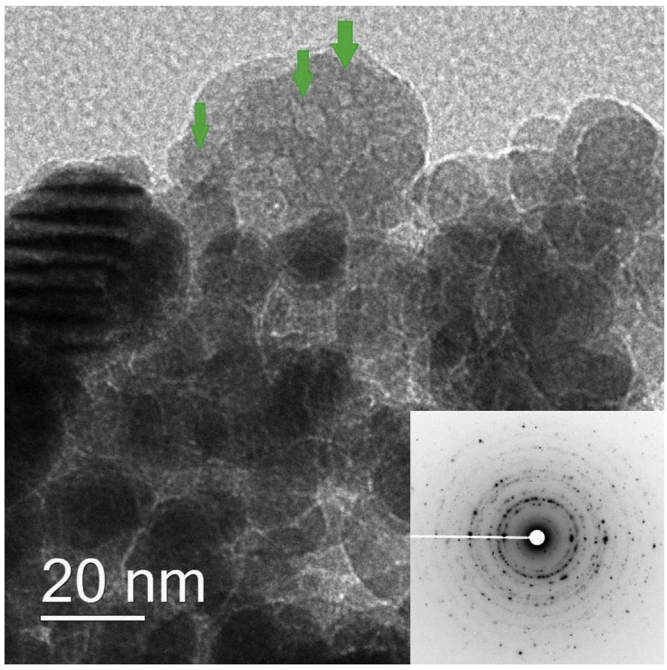

Fig. 4. Bright field TEM image showing crystalline particles 10–50 nm in diameter. Extensive 2–5 nm diameter porosity is evident within the larger particles (green arrows). The electron diffraction pattern (inset) shows spacings consistent with magnetite Fe_3O_4. (For interpretation of the references to colour in this figure legend, the reader is referred to the web version of this article.)

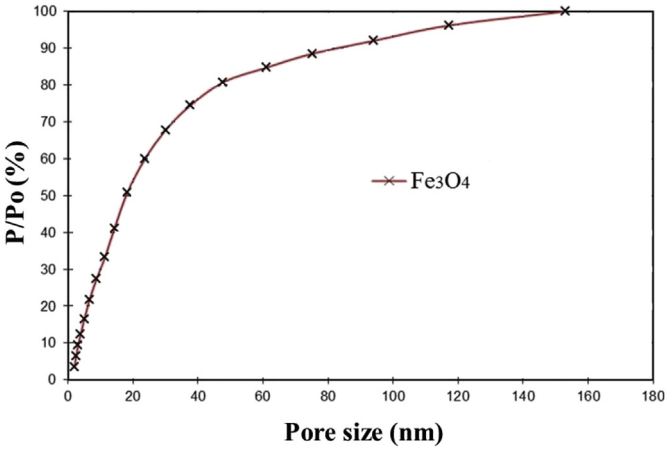

Fig. 5. Capillary hysteresis of nitrogen in pores of Fe_3O_4 at 77 K.

literature [32] aromatic hydrocarbons produce absorptions peaks in the regions 1600–1585 cm^{-1} and 1500–1400 cm^{-1}. This is in very good agreement with the peaks observed here at 1585 cm^{-1} (C–C stretch in-ring), and 1495 cm^{-1} (C–C stretch in-ring). On the other hand, bands related to S=O vibration were observed at 1325 cm^{-1} (asymmetric stretching), and at 1327 cm^{-1} (stretching). The bands in the region between 3415 and 3473 cm^{-1} were associated with the stretching vibrations of water molecules (O–H). It is clear from FT-IR analysis that methyl blue dye can be adsorbed on the surface of a Fe_3O_4 porous structure. A pure Fe_3O_4 sample without exposure to methyl blue showed only bands related to vapour water in region between 1000 and 1250 cm^{-1}, and for CO_2 at 2360 cm^{-1}. The strong absorption band just at the edge of the sensitivity window of the spectrometer at ~590 cm^{-1} was the ν_1 vibrational mode of Fe–O [28,30], observed for all metal-oxide bonds (Fig. 9).

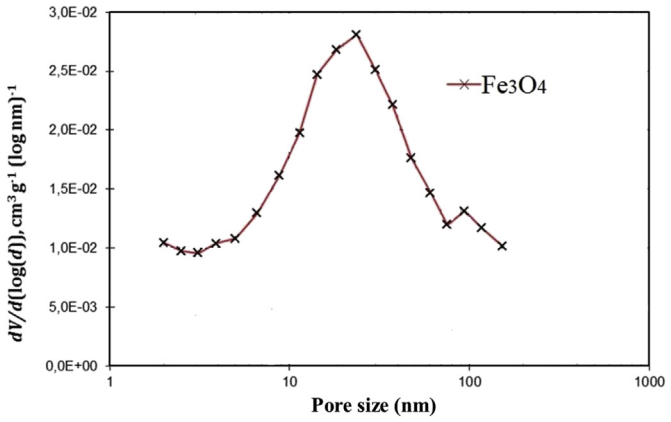

Fig. 6. The pore size distributions of Fe_3O_4 calculated from adsorption–desorption branches of nitrogen isotherms.

3.6. UV–visible analysis

Fig. 10 shows the absorbance of light passing through a bottle containing water and porous Fe_3O_4 with adsorbed methyl blue, as a functions of time after application of a combined AC/DC magnetic fields (AC, f = 10 Hz), and a DC field only for periods between 1 and 60 min Fig. 11 shows the equivalent plot for an applied AC field only.

The intensity of the absorption peak at 580 nm increases with the time after which the AC/DC field, and AC fields only were applied, due to increased concentration of methyl blue released into the water. The effect of an AC/DC field (Fig. 10) is greater than that of an AC field only (Fig. 11), by a factor of about two. The release of methyl blue to the water as a function of magnetic field type and time is shown in Fig. 12.

For the applied DC magnetic field only, no release of methyl blue was detected. With application of an AC field only, substantial absorbance due to methyl blue was detected even when the field was applied for just 1 min. Longer exposure to an AC field resulted in an increased absorbance, although the rate of increase had begun to taper off at 60 min. This effect was seen with magnetic field frequencies as low as 1 Hz (not shown), but higher frequencies resulted in a faster release of methyl blue. However, when both DC and AC magnetic fields were applied simultaneously the release of methyl blue was faster than with the AC field only (Figs. 10–12).

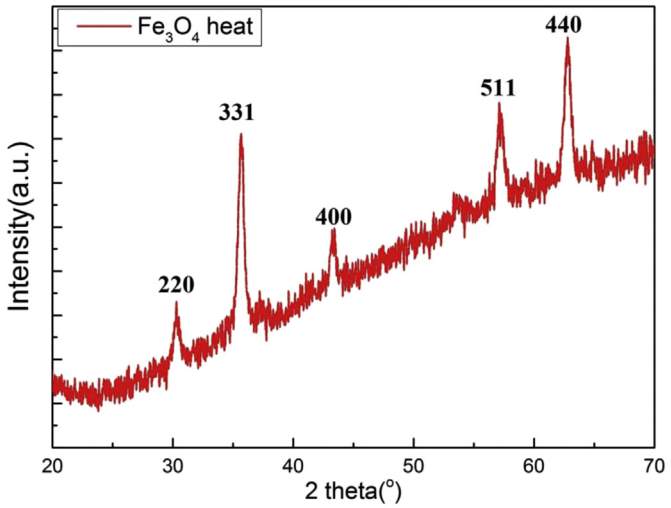

Fig. 7. XRD pattern of porous Fe_3O_4.

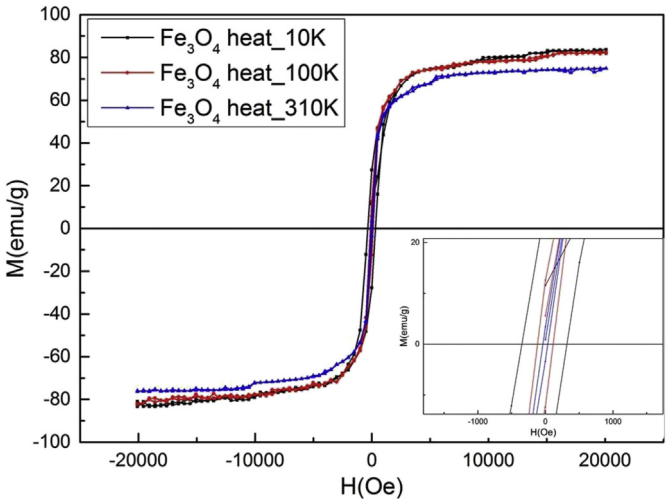

Fig. 8. The magnetic hysteresis loops of porous Fe_3O_4 at temperatures of 10, 100, and 310 K. The zoomed low-field region (inset) shows values of the coercive field.

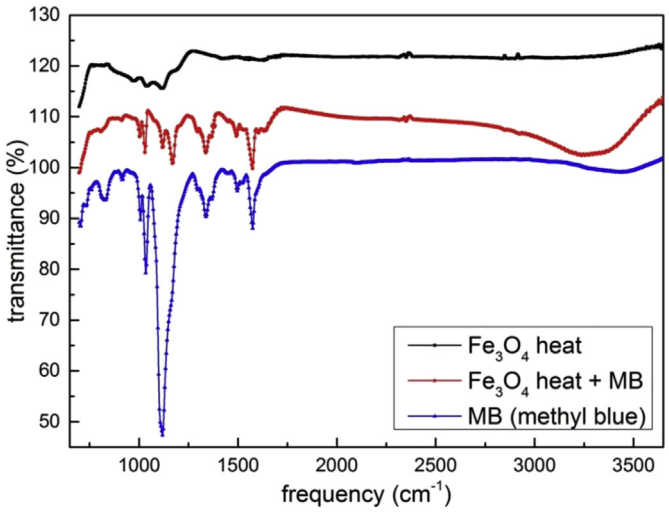

Fig. 9. FTIR spectra of as-prepared porous Fe_3O_4, porous Fe_3O_4 after exposure to methyl blue, and methyl blue.

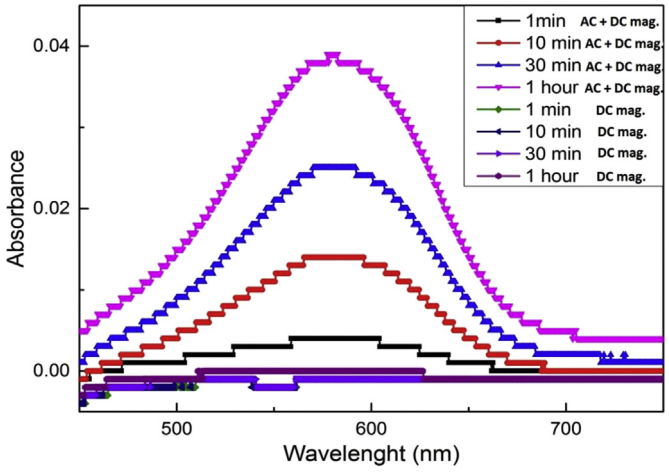

Fig. 10. Absorbance of light passing through water into which methyl blue is released from Fe_3O_4 nanostructures upon application of combined AC/DC magnetic fields (f = 10 Hz), and DC magnetic field only. The field was applied for periods of between 1 and 60 min.

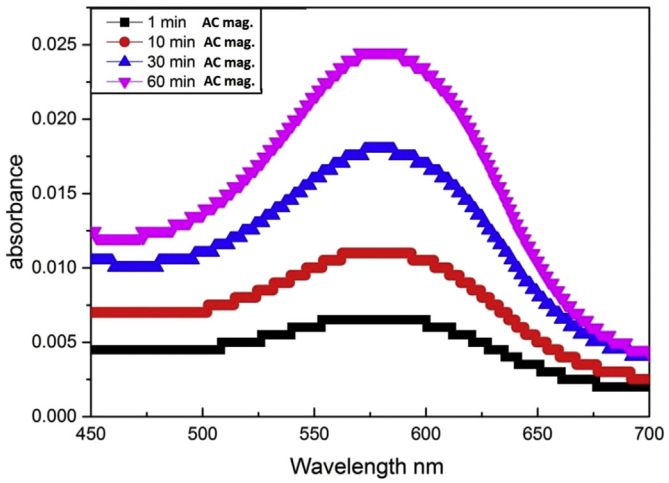

Fig. 11. Absorbance of light passing through water into which methyl blue is released from Fe_3O_4 nanostructures upon application of AC magnetic field (f = 10 Hz). The field was applied for periods between 1 and 60 min.

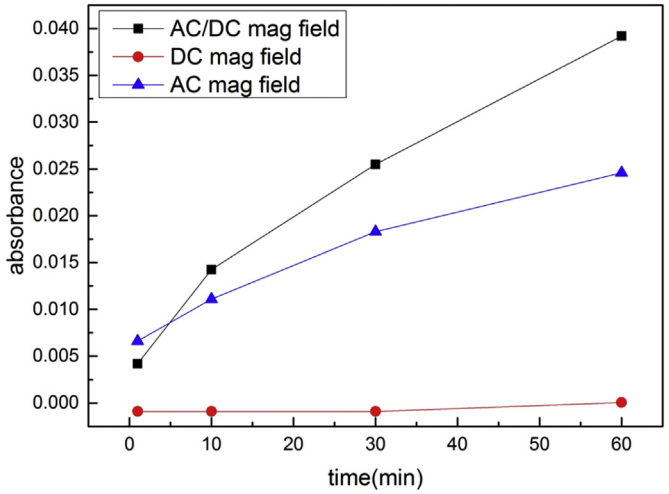

Fig. 12. Influence of magnetic field type on the release of MB as a function of time AC (blue triangles), combined AC/DC (black squares), and DC only (red circles). (AC fields are 10 Hz). (For interpretation of the references to colour in this figure legend, the reader is referred to the web version of this article.)

The response of the system to low frequency AC fields helped explain the mechanism of the release of methyl blue. Direct visual inspection of the magnetic nanopowder in the water showed that the application of an AC only field resulted in barely visible movement of the Fe_3O_4 nanopowder which settled at the bottom of the bottle.

However, application of a DC field using an Nd–B–Fe magnet near the bottle caused the Fe_3O_4 nanopowder to line up forming filaments at the bottom of bottle (Fig. 13c–e).

These filaments vibrated when an AC magnetic field was also applied. This movement of Fe_3O_4 nanostructures in water is responsible for the release of methyl blue.

Application of a DC field only did not stimulate release of MB, as the nanopowder did not move. The permanent magnetic field kept the dye enclosed in the magnetic material, disabling the usual vibrations of particles in the fluid (water) caused by the kinetics of molecules of water.

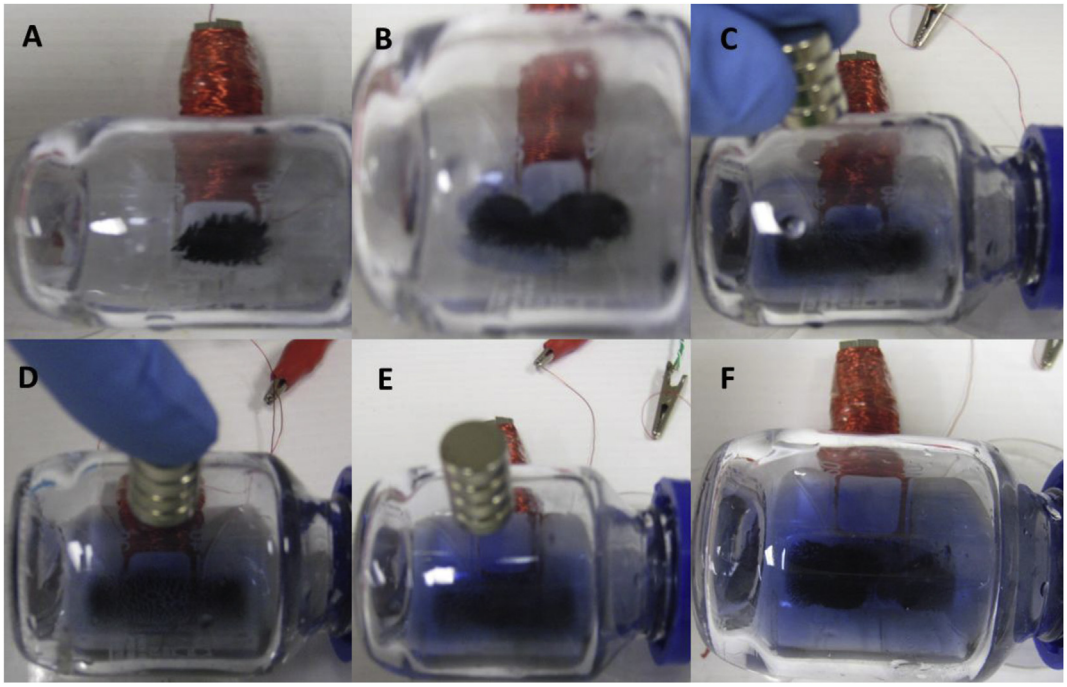

Fig. 13. A photo of the hybrid magnets setup in time lapse. a) shows nanopowder before application of any magnetic fields; b) presents nanopowder for only AC applied; c),d),e) show nanopowder for applied both AC and DC magnetic fields.

Importantly, the application of an AC field only resulted in a slow release of MB, affecting only small number of nanopowder in the area of separation line between the two poles, with much less obvious amplitude of oscillation (video 1). In contrast, when a combined AC/DC field was applied, particle alignment (agglomeration) in filaments induced by the DC field greatly increased the particle oscillation, and release occurred uniformly in the whole area due to the effects of the AC field (videos 2, 3, 4).

Supplementary data related to this article can be found online at http://dx.doi.org/10.1016/j.micromeso.2015.12.032.

As can be seen from our experimental data (Fig. 12) the combined AC and DC magnetic fields released 40% more dye than with the AC field only, and a negligible amount of dye was released when the DC field of a permanent magnet was applied.

We attribute the release behaviour of this material to be a result of the friction between oscillating particles and fluid (water), and friction between the aligned particles. A DC field causes alignment of particles, but no vibration, and thus causes negligible release. A pure AC field causes particles to oscillate and frictional interactions with neighbouring particles, causes some release. However, the particles are not strongly bound together, and so these interactions are not strong and affect a limited number of particles. The application of a combined DC and AC field results in both strong alignment (bonding) and oscillations. This greatly increases the frictional interactions between the particles themselves and between particles and the fluid (water) as well, leading to the highest release rate of methyl blue.

To test how much of MB can be loaded into the porous Fe_3O_4, 2.35 mg of MB was diluted in 50 ml of deionised water. 8.23 mg of porous Fe_3O_4 was added into equivalent second solution. Both solutions were left standing for 24 h. Measurements of the absorption coefficient in visible light for both solutions showed that 0.48 mg of MB was withdrawn from the water solution by porous Fe_3O_4. This implies that the Fe_3O_4 absorbed 6 wt% of MB.

4. Conclusions

A simple candidate drug delivery system using porous Fe_3O_4 has been trialled. Methyl blue has been used as a surrogate drug, due to the convenience of monitoring its release photometrically. Fe_3O_4 is biocompatible, obviating the need for barrier coatings which might impact on the drug take-up and release performance. DC fields alone cause particle alignment, but no release. AC fields induced modest release. However, the greatest release occurred in the presence of a combined AC and DC field. We attribute the release process to be due to frictional interactions among particles by themselves, and particles and fluid (water), as they oscillate in an AC field. The enhanced release observed in a combined AC/DC field regime is due to increased interaction between oscillating particles as a result of alignment in the DC field. A list of potential advantages and disadvantages of this approach is given below.

Advantages of the AC/DC setup as a drug delivery system:

1) Simple set up, one permanent magnet, one AC magnet which can be readily aligned with various human body parts.
2) Maximal drug release induced by combined AC/DC field, enabling highly localised delivery.
3) Strong release performance even at very modest magnetic field strengths.
4) The drug delivery system is chemically simple and easy to synthesise and control.
5) Good biological compatibility of the delivery and release systems.
6) Considerable potential for chemical and structural refinement to improve performance.

Disadvantages of the DC/AC of the AC/DC setup as a drug delivery system:

1) Difficulties in removing porous material (particles) from the human body.
2) Precise release of drugs is challenging within the larger parts of human body such as the abdominal cavity, thorax, and skull.

Acknowledgements

This work was also supported by the Australian Research Council (Grant no. DE130101247). The help of Prof Shi Xue Dou at ISEM is gratefully acknowledged.

References

[1] V.P. Torchilin, V.S. Trubetskoy, K.R. Whiteman, P. Caliceti, P. Ferruti, F.M. Veronese, J. Pharm. Sci. 84 (1995) 1049–1053.
[2] V. Weissig, K.R. Whiteman, V.P. Torchilin, Pharm. Res. 15 (1998) 1552–1556.
[3] P.K. Working, M.S. Newman, T. Sullivan, J. Yarrington, J. Pharmacol. Exp. Ther. 289 (1999) 1128–1133.
[4] M. Jahanshahi, Z. Babaei, Afr. J. Biotech. 7 (2008) 4926.
[5] F. Yuan, Semin. Radiat. Oncol. 8 (1998) 164–175.
[6] J.F. Kukowska-Latallo, K.A. Candido, C. Zhengyi, S.S. Nigavekar, I.J. Majoros, T.P. Thomas, L.P. Balogh, M.K. Khan, J.R. Baker Jr, Cancer Res. 65 (2005) 5317.
[7] U. Schroeder, P. Sommerfeld, S. Ulrich, B.A. Sabel, J. Pharm. Sci. 87 (1998) 1305–1307.
[8] J. Kreuter, Adv. Drug Deliv. 47 (2001) 65–81.
[9] O.C. Farokhzad, J. Cheng, B.A. Teply, et al., Proc. Natl. Acad. Sci. U. S. A. 103 (2006) 6315–6320.
[10] H.S. Yoo, K.H. Lee, J.E. Oh, T.G. Park, J. Controll. Release 68 (2000) 419–431.
[11] M. Yokoyama, M. Miyauchi, N. Yamada, T. Okano, Y. Sakurai, K. Kataoka, S. Inoue, Cancer Res. 50 (1990) 1693–1700.
[12] J. Chatterjee, Y. Haik, C.J. Chen, J. Magn. Magn. Mater. 225 (2001) 21–29.
[13] B. Bittner, B. Ronneberger, R. Zange, C. Volland, J.M. Anderson, T. Kissel, J. Microencapsul. 15 (1998) 495–514.
[14] K. Paal, J. Muller, L. Hegedus, Eur. J. Biochem. 268 (2001) 2187–2191.
[15] D. Le Garrec, J. Taillefer, J.E. Van Lier, V. Lenaerts, J.C. Leroux, J. Drug Target 10 (2002) 429–437.
[16] T. Wang, V.A. Petrenko, V.P. Torchilin, Mol. Pharm. 7 (4) (2010) 1007–1014.
[17] H.S. Yoo, E.A. Lee, T.G. Park, J. Controll. Release 82 (2002) 17–27.
[18] H. Li, Z. Lu, G. Cheng, K. Rong, F. Chena, R. Chen, RSC Adv. 5 (2015) 5059–5067.
[19] M. Mustapić, D. Pajić, N. Novosel, E. Babić, K. Zadro, M. Cindrić, J. Horvat, Ž. Skoko, M. Bijelić, A. Shcherbakov, Croat. Chem. Acta 83 (2010) 275–282.
[20] A. Akbarzadeh, H. Mikaeili, N. Zarghami, R. Mohammad, A. Barkhordari, S. Davaran, Int. J. Nanomedicine 7 (2012) 511–526.
[21] Y. Nakayama, M. Mustapić, H. Ebrahimian, P. Wagner, J.H. Kim, Md Sh, Al Hossain, J. Horvat, B. Martinac, Eur. Biophys. J. 44 (2015) 647–654.
[22] Z. Huang, F. Li, B.g Chena, G. Yuan, RSC Adv. 5 (2015) 14027–14033.
[23] S. Brunauer, P.H. Emmett, E. Teller, J. Am. Chem. Soc. 60 (1938) 309.
[24] E.P. Barrett, L.G. Joyner, P.P. Halenda, J. Am. Chem. Soc. 73 (1951) 373–380.
[25] M. Mustapić, J. Horvat, M.S. Hossain, Ž. Skoko, S.X. Dou, Acta Mater. 70 (2014) 298–306.
[26] M. Mustapić, J. Horvat, M.S. Hossain, Ž. Skoko, S.X. Dou, Supercond. Sci. Technol. 26 (2013) 075013.
[27] H. El Ghandoor, H.M. Zidan, Mostafa M.H. Khalil, M.I.M. Ismail, Int. J. Electrochem. Sci. 7 (2012) 5734–5745.
[28] L.-H. Shen, J.-F. Bao, D. Wang, Y.-X. Wang, Z.-W. Chen, L. Ren, X. Zhou, X.-B. Ke, M. Chena, A.-Q. Yanga, Nanoscale 5 (2013) 2133.
[29] P.L. Hariani, M. Faizal, R. Marsi, D. Setiabudidaya, Int. J. Environ. Sci. Dev. 4 (2013) 3.
[30] J. Sun, S. Zhou, P. Hou, Y. Yang, J. Weng, X. Li, M. Li, J. Biomed. Mater. Res. Part A 80A (2) (2007) 333–341, http://dx.doi.org/10.1002/jbm.a.30909.
[31] W. Wu, Q. He, C. Jiang, Nanoscale Res. Lett. 3 (2008) 397–415.
[32] C. Pouchert, Aldrich Library of Infrared Spectra, third ed., Aldrich Chemical Co., 1981, p. 1850.